JOC The Journal of Organic Chemistry

Article

pubs.acs.org/joc

Structural Studies of Supramolecular G-Quadruplexes Formed from 8-Aryl-2′-deoxyguanosine Derivatives

Marilyn García-Arriaga, Gerard Hobley, and José M. Rivera*

Department of Chemistry and Molecular Sciences Research Center, University of Puerto Rico at Río Piedras, San Juan, Puerto Rico 00926, United States

Supporting Information

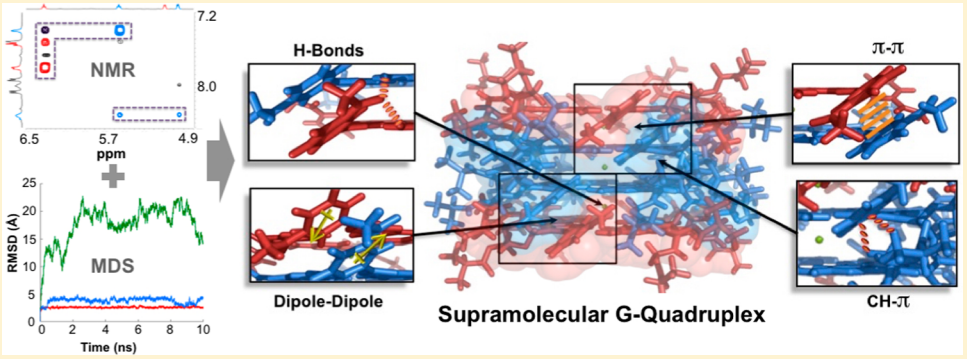

ABSTRACT: Self-assembly is a powerful tool for the construction of complex nanostructures. Despite advances in the field, the development of precise self-assembled structures remains a challenge. We have shown that, in the presence of suitably sized cations like K^+, 8-aryl-2′-deoxyguanosine (8ArG) derivatives self-assemble into sets of coaxially stacked planar tetramers, which we term supramolecular G-quadruplexes (SGQs). Previously, we reported that, when the 8-aryl group is a phenyl ring with a meta-carbonyl group, the resulting supramolecule is a hexadecamer, which is remarkably robust as illustrated by its isostructural assembly in both organic and aqueous environments. We report here a detailed three-dimensional structure of the SGQs formed by lipophilic, and hydrophilic, 8ArG derivatives with either 8-(meta-acetylphenyl), 8-(para-acetylphenyl), or 8-(meta-ethoxycarbonylphenyl) groups. The chirality and close contacts between the subunits impose different levels of steric and electrostatic constraints on opposite sides of the tetrads, which determine their preferred relative orientation. The balance between attractive noncovalent interactions juxtaposed with repulsive steric and electrostatic interactions explains the high cooperativity, fidelity, and stability of these SGQs. These structural studies, together with titration experiments and molecular dynamics simulations, provide insight into the mechanism of formation of these SGQs.

INTRODUCTION

Self-assembly provides a powerful strategy for the construction of functional nanostructures. Self-assembled supramolecules can be broadly classified into two categories: closed and open structures.[1,2] The former are characterized by forming two-dimensional or three-dimensional macrocycles that are generally discrete due to their inherent geometric or topological constraints.[3] On the other hand, open structures are generally polymeric in nature and are of indefinite size in at least one dimension. Linear, one-dimensional assemblies are those with high aspect ratios such as those found in liquid-crystals,[4−7] self-assembled nanotubes or nanofibers,[8−11] and supramolecular polymers.[6,12−18] Controlling the size of both natural and synthetic one-dimensional open supramolecules can be achieved by modulating the concentration and/or temperature of the subunits,[17] by introducing electrostatic repulsion,[15,16,19] or by the addition of capping agents.[20,21]

How can the subunits in a supramolecule be programed with the appropriate self-termination information? It is attractive to develop subunits that self-assemble into discrete and well-defined one-dimensional supramolecules via a self-terminating mechanism. For homomeric assemblies, this can be achieved by using asymmetric subunits that show a preferential association in one direction (i.e., anisotropic assembly), together with negative cooperative effects that discourage further growth after reaching a certain threshold size.[22]

Guanine (G) and derivatives thereof are known to self-assemble into planar tetramers or tetrads (T) that stack in the presence of cations into supramolecular G-quadruplexes (SGQs).[23−27] Guanine derivatives can form SGQs that range in size from a two-tetrad (2T-SGQ or octamer)[28] assembly to columnar aggregates containing an indefinite number of tetrads.[29] The sizes of such SGQs have been modulated by controlling the concentration of the constituent subunits or by changing the cation templates.[30] The Davis group has also reported that a 4T-SGQ or hexadecamer could be form via the putative picrate-mediated dimerization of two octamers.[27]

Received: May 11, 2016
Published: June 15, 2016

DOI: 10.1021/acs.joc.6b01113
J. Org. Chem. 2016, 81, 6026−6035

We have developed an alternative approach toward modulating the structure of SGQs that relies in replacing the H8 in the guanine moiety with a functionalized phenyl group.[31] The position of the functional group on the phenyl ring enables modulation of the molecularity and stability (thermal and kinetic) of the resulting supramolecules. For example, in the presence of potassium cations the mAG (*meta*-acetylphenyl) scaffold promotes the formation of a four-tetrad (4T) SGQ or hexadecamer in both organic and aqueous environments.[32] Furthermore, such 4T-SGQ are isostructural and self-assemble with high fidelity and stability.[33] In contrast, the isomeric derivative **3** (*para*-acetylphenyl) leads the formation of 2T-SGQs or octamers (Figure 1).[31] Herein we report NMR spectroscopic and molecular dynamics simulation (MDS) studies to determine the three-dimensional structure of various 4T-SGQs, in order to provide a detail molecular level explanation for these phenomena. We show that the balance between attractive and repulsive interactions is responsible for the self-terminating behavior and high stability of these supramolecules. Furthermore, these structures suggest a possible mechanism of formation for these supramolecules.

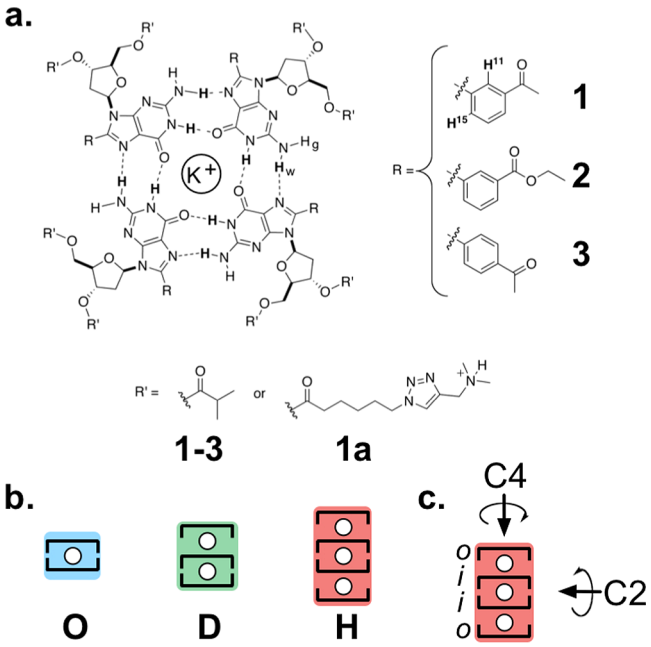

Figure 1. (a) Chemical structure of the "all-*syn*" tetrads formed by **1**, **1a**, **2**, and **3**. (b) Cartoon depiction for the various *n*T-SGQs mentioned in this article: octamer (2T-SGQ, blue); dodecamer (3T-SGQ, green); and hexadecamer (4T-SGQ, red). (c) Schematic depiction of the main axes of symmetry and the labeling of the two types of tetrads, inner (i) and outer (o), for the 4T-SGQ. The letters w and g, in $N2H_w$ and $N2H_g$, denote the Watson–Crick and groove edges of the tetrad.

RESULTS AND DISCUSSION

NMR Studies. NMR spectroscopy has previously been used for the structural elucidation of SGQs in organic media. In 1999, Gottarelli and colleagues elucidated the structure of an octamer formed by a lipophilic guanosine derivative, composed of two tetramers one "all-*anti*" and another "all-*syn*" in a head-to-tail (*ht*) orientation.[41,42] Later, the groups of Davis, Gottarelli, and Spada reported the NMR based structural elucidation of a self-assembled tubular polymeric structure based on a related lipophilic guanosine derivative.[27] Furthermore, the groups of Davis and Meijer reported various crystal structures of hexadecameric lipophilic guanosine derivatives.[19,43,44] The former, reported the formation of an "all-*anti*" D_4 symmetric *ht-hh-th* hexadecamer containing a mixture of K^+ and Cs^+ while the latter contained only potassium picrate in CH_3CN.[43,44] Subsequently, González-Rodríguez and Meijer reported an identical 3D organization although they used THF as the solvent.[19] Changing the counteranion, however, from picrate to KPF_6 resulted in a slow (a few days) shift from the D_4 symmetry *ht-hh-th* hexadecamer to a C_4 symmetry *hh-th-th* hexadecamer. All the reported structures to this date point towards the fact that the favored supramolecular configuration for hexadecamers made from lipophilic guanosine derivatives is D_4 symmetric with the *ht-hh-th* interfaces.

NMR spectroscopy was used to characterize the SGQ formed by **1** in organic media. The addition of KI to a solution of **1** in CD_3CN promotes its self-assembly leading to a dramatic change in the ^1H NMR spectrum (Figure 2; Table 1). Titration of a solution of **1** with incremental amounts of KI enables the identification of key intermediates in the self-assembly pathway as described further below in this article. However, having an excess of KI (0.5 equiv relative to **1**) shifts the equilibrium toward the formation of a 4T-SGQ ($\mathbf{1}_{16}$), enabling the well-resolved 1D/2D NMR spectra necessary to perform the rigorous analysis required to determine the structure with atomic resolution. The average hydrodynamic radius and molecular weight for $\mathbf{1}_{16}$ as determined, respectively, by DOSY NMR and VPO are 10.0 Å and 8661 g/mol.

The 1D and 2D NMR data are consistent with a structure composed of four distinct tetrads displaying D_4 symmetry (Figure 1c). The ^1H NMR spectrum for $\mathbf{1}_{16}$ shows two sets of signals in a 1:1 ratio indicating that each tetrad is composed of four molecules of **1** in two different chemical environments (i.e., for the outer and inner tetrads) as expected for a system of D_4 symmetry (Figure 1c; Figure 2).[45] The correlations within the same tetrad (intratetrad) were determined by 2D COSY cross-peaks, enabling the identification of the protons corresponding to the inner and the outer tetrads. The chemical shifts for the exchangeable and nonexchangeable protons of **1** are listed in Table 1.

Structural Model. The 3D structure of $\mathbf{1}_{16}$ was assessed starting from the crystal structure of nonesterified precursor of **1**. From the crystallographic data, the dihedral angle (O4′–C1′–N9–C4) between ribose–base and the base–phenyl (C10–C15–C8–N7) were determined to be 59° and 33°, respectively (Figure 3a; Table S1–S5). The former corresponds to the *syn* conformation characteristic of guanosine derivatives substituted at C8,[46] which causes the bulk of ribose moiety to be slightly shifted toward the head (*h*) of the resulting "all-*syn*" tetrad (Figure 3b).

The fact that the subunits are "locked" in the *syn* conformation minimizes the possible configurations of the resulting SGQs leaving only three possible orientations available (*hh*, *ht*, and *tt*) for any given pair of tetrads (Figure 4). Since the NMR spectra corresponds to a 4T-SGQ structure of D_4 symmetry, only the four configurations depicted in Figure 4c are possible. The next step to solve the structural puzzle was to evaluate 2D NOESY spectra described below.

NOE Assignments. The intratetrad NOEs are key for the determination of the orientation of the phenyl ring and the acetyl group. NOEs of the aromatic region of the spectra reveal interactions between the H1′i–H11i of the inner tetrads and

DOI: 10.1021/acs.joc.6b01113
J. Org. Chem. 2016, 81, 6026–6035

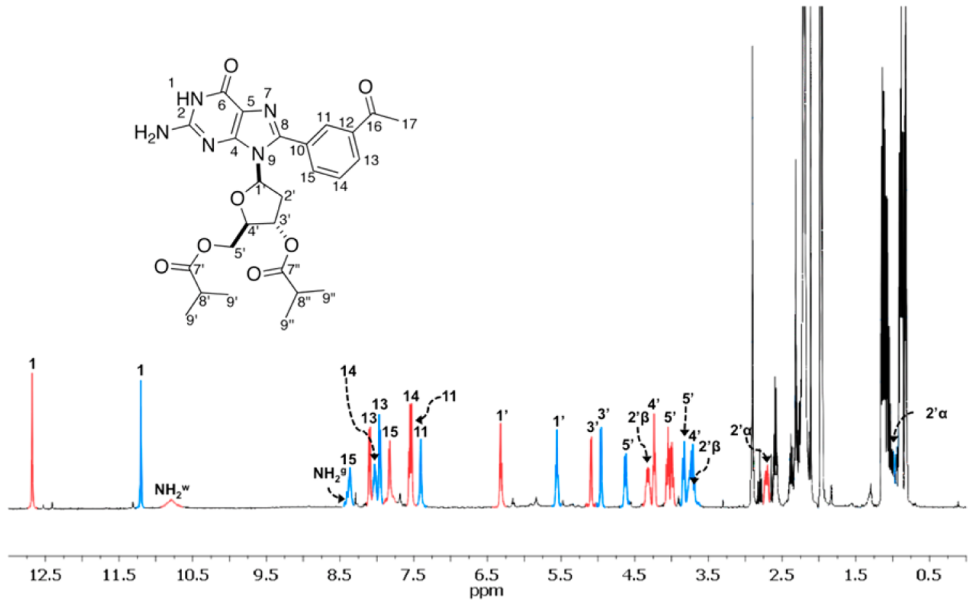

Figure 2. ^{1}H NMR of $\mathbf{1}_{16}$ (30 mM in **1**; 0.5 equiv KI) in CD_3CN. The peaks corresponding to the inner and outer tetrads are colored in blue and red, respectively.[47]

Table 1. ^{1}H NMR Chemical Shifts for the Guanine and the Ribose Moieties in $\mathbf{1}_{16}$ for the Spectrum Shown in Figure 2

	NH1	NH2	H1′	H2′α	H2′β	H3′	H4′	H5′/ H5″[a]
o	12.68	10.79	6.32	2.71	4.33	5.09	4.24	4.05/3.99
i	11.20	7.78	5.55	0.99	3.75	4.95	3.71	4.62/3.84

[a]Not differentiated.

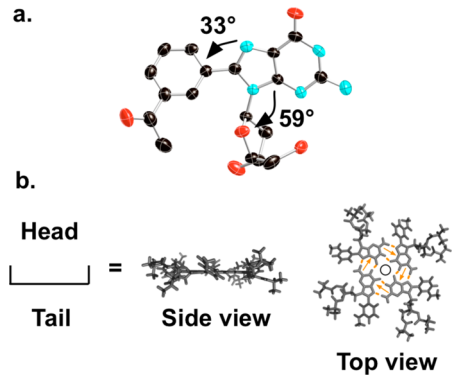

Figure 3. (a) Dihedral angles of the glycosydic bond and the phenyl moiety, as obtained by the crystal structure of the nonesterified precursor of **1**. (b) Side and top views of a molecular model for a tetrad with a schematic representation of the former. The direction of the hydrogen bond donors on the Watson−Crick edge is indicated by orange arrows, which are use to distinguish the two diastereomeric faces of the tetrad. The head (*h*) of the tetrad is defined when the rotation is clockwise and the opposite side is denoted as the tail (*t*).

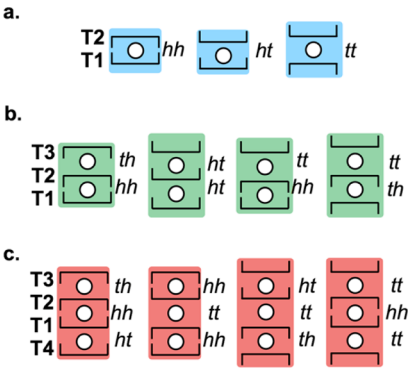

Figure 4. Potential configurations for the various *n*T-SGQs discussed in this study. (a) Two possible 2T-SGQ (octamers) of D_4 symmetry; (b) four possible 3T-SGQ (dodecamers); (c) four possible 4T-SGQ (hexadecamers) of D_4 symmetry. The tetrads T1-T4 are numbered according to the proposed order in which they are added to SGQs of increasing size. For 4T-SGQs, T1/T2 and T3/T4 are alternatively referred to as inner and outer tetrads, respectively.

the H14o/H15o−H1′o of the outer tetrads (Figure 5). The lack of interactions between H13o and H14o with NH1 and/or $N2H_w$ and H11o with H1′o leads us to conclude that the dihedral angle of the phenyl ring in the outer tetrads should be around 40° (Figure 3). Although we can observe cross-peaks indicating inner tetrad interaction between H1′i−H11i, the lack of interactions among the other protons from the phenyl and the ribose rings supports a semi perpendicular arrangement of the guanine-phenyl dihedral angle of 139.5°.

The assignment of the intertetrad NOEs correlations are key to reveal the tetrads' relative stereochemical orientation with respect to their two (*h*, *t*) diastereotopic faces (Figure 3b). The interaction between H15i−H2′βi is key to elucidate the relative orientation of the two inner tetrads (Figure 6). The correlation between H11i−H2′o indicates that H11i is pointing towards the outer tetrad (Figure 7), which in turn pushes the H15i toward the center of the hexadecamer, this serves to corroborate that the H15i−H2′βi corresponds to an intertetrad NOE (Figure 6). These interactions between the hexadecamer's inner tetrads suggests their origin as the precursor *hh*

DOI: 10.1021/acs.joc.6b01113
J. Org. Chem. 2016, 81, 6026−6035

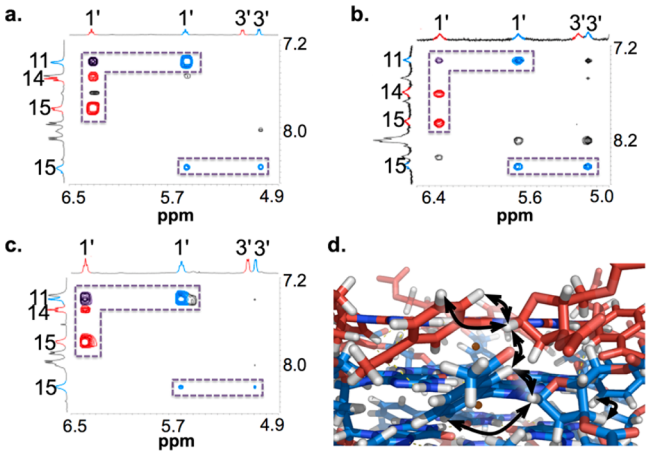

Figure 5. NOESY signature correlations between the protons in the aromatic and the deoxyribose (H1′ and H3′) regions. Both $\mathbf{1}_{16}$ (a) and $\mathbf{2}_{16}$ (c) are in CD_3CN while $(\mathbf{1a})_{16}$ (b) is in H_2O–D_2O (9:1). (d) Close up of the molecular model of $\mathbf{1}_{16}$ where the double-headed arrows indicate the corresponding correlations presented in a–c.

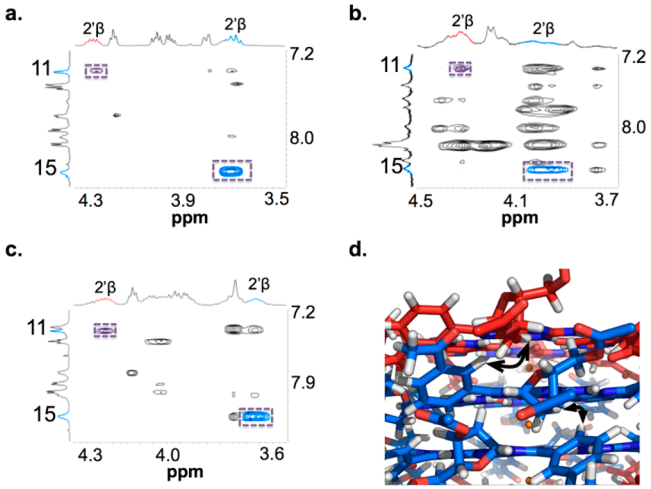

Figure 6. NOESY signature correlations between the protons in the aromatic and the deoxyribose (H2′ and H4′) regions. Both $\mathbf{1}_{16}$ (a) and $\mathbf{2}_{16}$ (c) are in CD_3CN while $(\mathbf{1a})_{16}$ (b) is in H_2O–D_2O (9:1). (d) Close up of the molecular model of $\mathbf{1}_{16}$ where the double-headed arrows indicate the corresponding correlations presented in a–c.

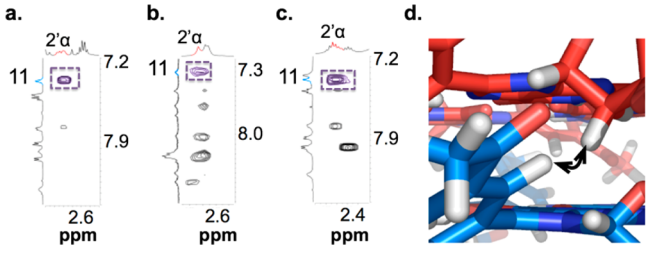

Figure 7. NOESY signature correlations between the protons in the aromatic and the deoxyribose (H2′) regions. Both $\mathbf{1}_{16}$ (a) and $\mathbf{2}_{16}$ (c) are in CD_3CN while $(\mathbf{1a})_{16}$ (b) is in H_2O–D_2O (9:1). (d) Close up of the molecular model of 1_{16} where the double-headed arrows indicate the corresponding correlations presented in a–c.

octamer (2T-SGQ), which also provided the initial clue for the mechanism of formation for the SGQs.

Interactions between H1′o/H2′*α*o–H11i, 2H5′i/H4′i–H2′*β*o, and H1′i–H3′o (Figures 5, 7, S11) indicate a *ht* arrangement among the inner and outer tetrads, since the corresponding ribose oxygens point upward. The region corresponding to the hydrogen-bonded N1H in the NOESY spectrum is well resolved and reveals intertetrad NOEs between the base $N2H_wi$–$N2H_wo$ and $N2H_wo$/$N2H_go$–$N2H_gi$ (Figure 8).[47]

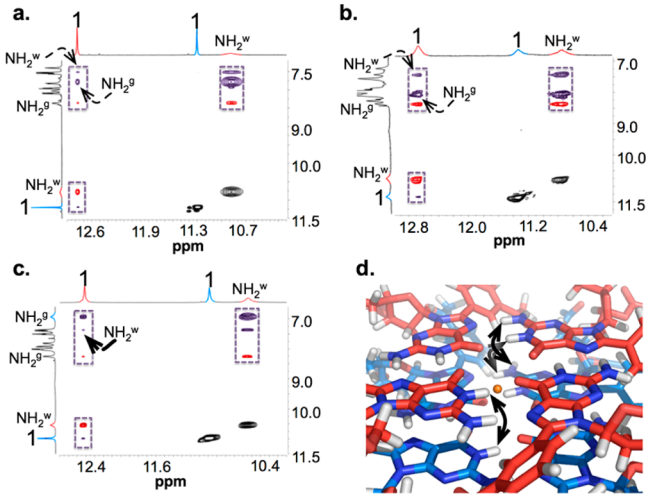

Figure 8. NOESY signature correlations between the protons in the aromatic and the guanine's N1H regions. Both $\mathbf{1}_{16}$ (a) and $\mathbf{2}_{16}$ (c) are in CD_3CN while $\mathbf{1a}_{16}$ (b) is in H_2O–D_2O (9:1). (d) Close up of the molecular model of 1_{16} where the double-headed arrows indicate the corresponding correlations presented in a–c.

The 2D NMR spectra is consistent with a structure in which the outer and inner tetrads approach each other via *ht* interface and the inner tetrads face each other via a *hh* interface, enabling a *ht-hh-th* 4T-SGQ. The *hh-tt-hh* 4T-SGQ isomer can be discarded because of the absence of the expected NOE signals. Furthermore, the model shows it to have enhanced steric hindrance between the phenyl rings at the outer-inner interface (Figure S3) and repulsive interactions between the corresponding ribose oxygens at the *tt* interface. The alternative *th-tt-ht* 4T-SGQ isomer, also lacks the expected NOE correlations in addition to presenting a repulsive parallel arrangement of the dipoles between the phenyl rings at the outer-inner interface (Figure S5).

The information obtained from the NOEs enabled the construction of the models for $\mathbf{1}_{16}$, $\mathbf{2}_{16}$ and $(\mathbf{1a})_{16}$ (Figure 9 and Figure S1).[32] The NOEs for all three of these 4T-SGQs are consistent with the *ht-hh-th* configuration and the correspond-

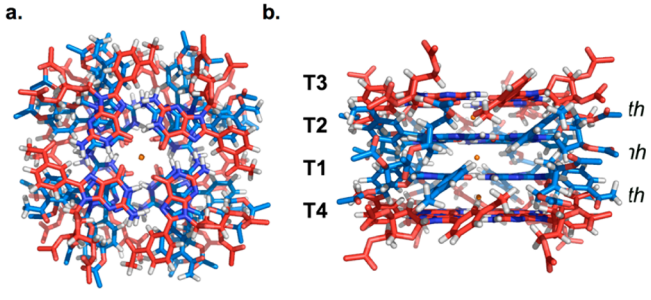

Figure 9. Molecular models for the 4T-SGQ formed by **1**. (a) Top and (b) side views of $\mathbf{1}_{16}$ where the inner and outer tetrads are colored in blue and red, respectively.

DOI: 10.1021/acs.joc.6b01113
J. Org. Chem. 2016, 81, 6026–6035

ing minimized models show no detrimental steric repulsions. Furthermore, unlike oligomeric G-quadruplexes (OGQs) where the backbone determines their relative twist between consecutive tetrads, SGQs have no such constraints and thus, the twist is dictated by the proper balance of attractive and repulsive noncovalent interactions.[26,48] The spectral data in combination with molecular modeling lead to intertetrad twist angles in the range of ~8°−10° (Figure S7).[49] These values deviate significantly from those independently reported by the groups of Davis[30] and Meijer[19] (based on the crystal structures of a related *ht-hh-th* 4T-SGQ), which were in the range of 17°−31°. This, however, should not be surprising given the additional steric restraints imposed by the 8-phenyl group, which prevents larger deviations in this particular parameter.

All the 4T-SGQs reported here have similar features, not only in the relative rotation between the tetrads, but also in the arrangement of the aryl and the ribose rings. This allowed us to identify a series of NOE correlations that serve as a fingerprint for the formation of 4T-SGQs (Figure 5). These signature correlations are present in all the 4T-SGQs formed by the *meta*-carbonyl derivatives reported in this article (**1**, **1a**, and **2**) as well as in 4T-SGQs of related derivatives like a "dendronized" version of **1** used to make self-assembled dendrimers.[50]

The fact that the 2T-SGQs observed in these studies are D_4−symmetric leaves only two possibilities for the relative arrangement of consecutive pairs of tetrads (*hh* or *tt*; Figure 4). This high symmetry, however, hampers the elucidation of the 2T-SGQ formed by the *para*-derivative **3** because all eight subunits in $\mathbf{3}_8$ are equivalent (Figure 10). We attempted to

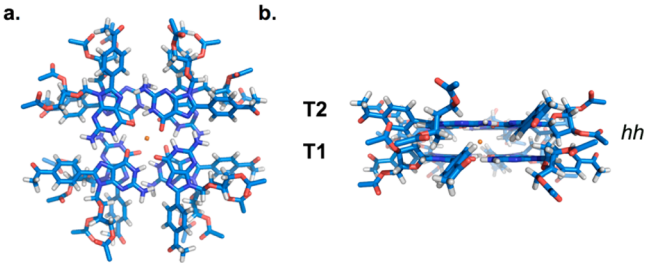

Figure 10. Molecular model for the 2T-SGQ formed by **3**; (a) top and (b) side views of $\mathbf{3}_8$.

overcome this obstacle by evaluating the corresponding 2T-SGQ formed by **2** in $CDCl_3$.[51] Although a *meta*-substituted phenyl group reduce the symmetry of $\mathbf{2}_8$ relative to $\mathbf{3}_8$, the resulting spectra (Figure S18−23) provided no meaningful additional information. We, thus, settled for a model constructed by removing the outer tetrads from the corresponding 4T-SGQ $\mathbf{1}_{16}$, moving the acetyl groups in **1** to the *para*-position to make **3**, and minimizing the resulting 2T-SGQ $\mathbf{3}_8$, which afforded the model shown in Figure 10.

Analysis of Noncovalent Interactions. A detailed analysis of the generated molecular models of 4T-SGQs reveal a number attractive noncovalent interactions (H-bonds, CH-π, π−π, and dipole−dipole) that operate in addition to those inherent in the SGQs not made from 8-aryl substituted guanosine derivatives (Figure 11). The presence of bifurcated H-bonds between the *meta*-acetyl groups from the outer tetrads (acceptors) with the $N2H_g$ (donors) from the inner tetrads was one of the most prominent noncovalent interactions identified from the resulting molecular models (Figure 11e). These bifurcated H-bonds enable the subunits in the outer tetrads to

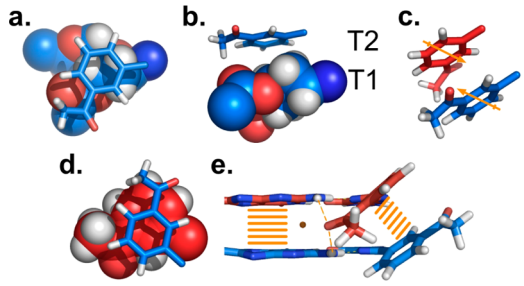

Figure 11. Representative noncovalent interactions between the 8Ar moieties that stabilize $\mathbf{1}_{16}$. (a) Top and (b) side views of attractive CH−π interactions between the eight subunits in T1 and T2. (c) Dipole−dipole interactions between the subunits in T1/T2 and T3/T4. (d) π−π interactions between the subunits in T1/T2 and T3/T4. (e) Bifurcated hydrogen bonds and π−π interactions between the subunits in T1/T2 and T3/T4. These interactions are new in 8ArG derivatives relative to the corresponding assemblies of the parent unmodified G.

be "clamped" in place, thus stabilizing this particular supramolecular configuration.

The resulting antiparallel arrangement of the dipoles between the phenyl rings of adjacent subunits in the inner/outer tetrads are also expected to stabilize the assembly. Furthermore, the electrostatic potential plots suggest that the contact surfaces of such adjacent subunits in the inner/outer tetrads have complementary electrostatic potentials (Figure 12),[52] which we hypothesize work synergistically with the dipole−dipole and π−π interactions.

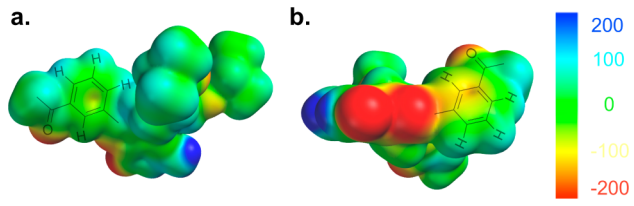

Figure 12. Molecular electrostatic potential plots (ESP) for the subunits of $\mathbf{1}_{16}$ in the (a) outer and (b) inner tetrads, indicating the two different faces of the phenyl ring.

Proposed Mechanism of Self-Assembly. Titration experiments of **1** with KI reveal below 0.1 equiv of the salt three main species are present in solution. One set of signals corresponds to the 4T-SGQ $\mathbf{1}_{16}$, which shows two sets of N1H signals at 11.20 and 12.68 ppm. The other two species correspond to the 2T-SGQ $\mathbf{1}_8$ and the 3T-SGQ $\mathbf{1}_{12}$ which show one and three sets of peaks, respectively (Figure 13a). The speciation curves constructed with the titration data (Figure 13b) reveal how in the first part of the titration a critical concentration of $\mathbf{1}_8$ is reached, after which it decreases while the formation of $\mathbf{1}_{12}$ becomes evident. The latter, however, never reaches a dominant proportion and it appears to represent a putative intermediate on the process of formation of $\mathbf{1}_{16}$. A dose-response curve of the percentage of the 4T-SGQ ($\mathbf{1}_{16}$) formed as a function of the log [KI] (Figure S16) leads to a Hill coefficient (n_H) of 5.0 ± 0.6 where its value greater than one is considered to be characteristic of a cooperative self-assembly.

The formation of the 2T-SGQ $\mathbf{1}_8$ corresponds to the first step of the assembly (Scheme 1) and given its D_4 symmetry, we can exclude that the dimerization of two octamers lead to the formation of the observed 4T-SGQ. The dimerization of two

DOI: 10.1021/acs.joc.6b01113
J. Org. Chem. 2016, 81, 6026−6035

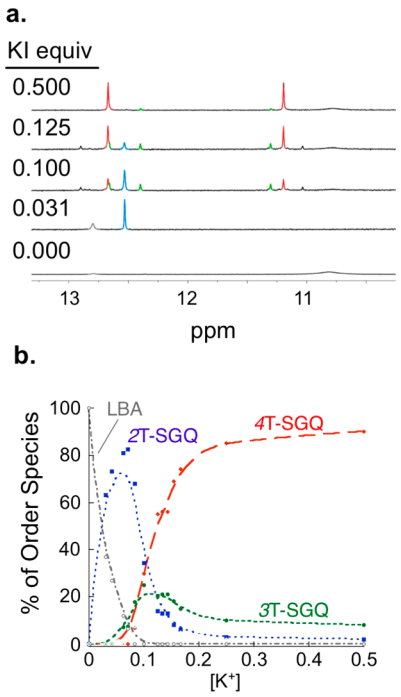

Figure 13. Titration of **1** (15 mM, in CD_3CN) with KI; (a) partial ^1H NMR spectra for the region corresponding to the N1H peaks; (b) speciation curves constructed from the data obtained from part (a). In both panels, the lines are color coded to represent 4T-SGQ (red), 2T-SGQ (blue), 3T-SGQ (green), and some loosely bound aggregates (LBA; gray).

Scheme 1. Proposed Mechanism of *n*T-SGQs Formed by 1[a]

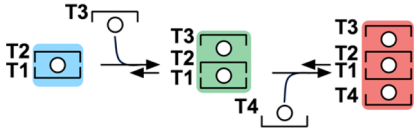

[a]Addition of K^+ (circle) promotes the formation of a 2T-SGQ (blue), while further incremental addition of K^+ favors the formation of a 4T-SGQ (red), forming a 3T-SGQ (green) as a metastable intermediate in the process.

D_4 2T-SGQs would result in a homomeric outer intertetrad interfaces (i.e., *hh-tt-hh* or *tt-hh-tt*). One can thus infer that the formation of a 4T-SGQ with heteromeric outer intertetrad interfaces (*ht-hh-ht*), like $\mathbf{1}_{16}$, involves the formation of a *hh* 2T-SGQ followed by the successive stacking of two tetrads at opposite ends of the structure (Scheme 1).

Our proposed mechanism also requires the transient formation of a 3T-SGQ intermediate, which is consistent with the titration data. For an assembly that starts from a *hh* 2T-SGQ the formation of the 3T-SGQ is limited to two possible isomers with intertetrad interfaces of *hh-th* or *hh-tt*. The latter alternative can be discarded due to the electrostatic repulsion imposed by the ribose oxygens at the *tt* interface. A *hh-th* 3T-SGQ in turn can produce only one 4T-SGQ of D_4 symmetry (*ht-hh-th*), which is the one we observe spectroscopically.

The proposed mechanism of self-assembly reveals why, despite SGQs being open assemblies, they do not continue to grow into indefinite columnar aggregates (Scheme 1). The model of $\mathbf{1}_{16}$ suggests that to form bifurcated H-bonds, the dipole of the phenyl ring for the incoming tetrad must by aligned with the phenyl ring of the outer tetrad, which results in repulsive interactions. Furthermore, molecular modeling analysis shows that the assembly of an incoming tetrad will result in an increase in steric hindrance of the system. Additional self-assembly studies with other *meta*-substituted derivatives show the formation of hexadecameric structures, when a carbonyl is present in this position.[53] This emphasizes the requirement of a carbonyl in the *meta*-position for the formation of a hexadecamer and highlights the importance of clamping the outermost subunits. The most prevalent species for *para*-substituted derivatives is the octameric 2T-SGQ. Further association of tetrads to $\mathbf{3}_8$ would result in the parallel alignment of the dipoles of the phenyl rings, which together with greater steric repulsion would destabilize the resulting supramolecule.

Molecular Dynamics Simulations. Molecular dynamics simulations (MDS) enable a deeper molecular level understanding of the self-assembly of 8ArGs to form SGQs and its time dependent evolution. Comparison of the NMR generated model of the 4T-SGQ and the final MD simulated structure lead to a RMSD of 0.636 Å (Figure S24). The very high concordance between both structures highlights the importance of the relatively rigid core in stabilizing the structure.

Analysis of the RMSD trajectory for the average structures of $\mathbf{1}_{16}$, $\mathbf{1}_{12}$, and $\mathbf{1}_8$ demonstrate that the former and the latter are the more stable assemblies, which agrees with the speciation curve (Figure 13b). The RMSD trajectory for $\mathbf{1}_{12}$ shows a drastic increment in structural fluctuations indicative of a significantly less stable assembly (Figure 14a). Both $\mathbf{1}_{16}$ and $\mathbf{1}_8$

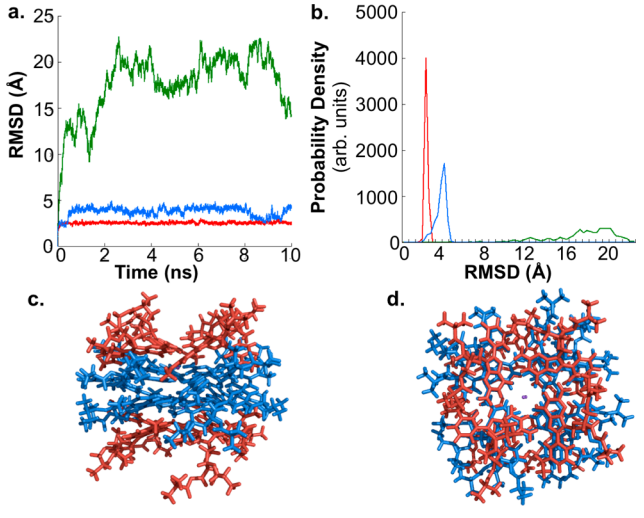

Figure 14. Dynamic behavior for three SGQs formed by **1**. (a) Evolution of the RMSD (relative to the NMR-based minimized structure) as a function of time and (b) its distribution for $\mathbf{1}_{16}$ (red), $\mathbf{1}_{12}$ (green), and $\mathbf{1}_8$ (blue). (c) Side and (d) top views of the final structure from the MDS of $\mathbf{1}_{16}$ with the inner and outer tetrads colored in blue and red, respectively.

have structural distributions peaks in the 2−4 Å range, with the former showing a narrower spread and lower RMSD average. This contrasts significantly from the one for $\mathbf{1}_{12}$, which has a wider structural distribution (Figure 14b). The fact that the 3T-SGQ $\mathbf{1}_{12}$ is never the major species, together with the apparent low stability suggested by the MDS, support its role as a metastable intermediate assembly. We have shown, however, that it is in fact possible to favor a 3T-SGQ with a related 8-(3-

DOI: 10.1021/acs.joc.6b01113
J. Org. Chem. 2016, 81, 6026−6035

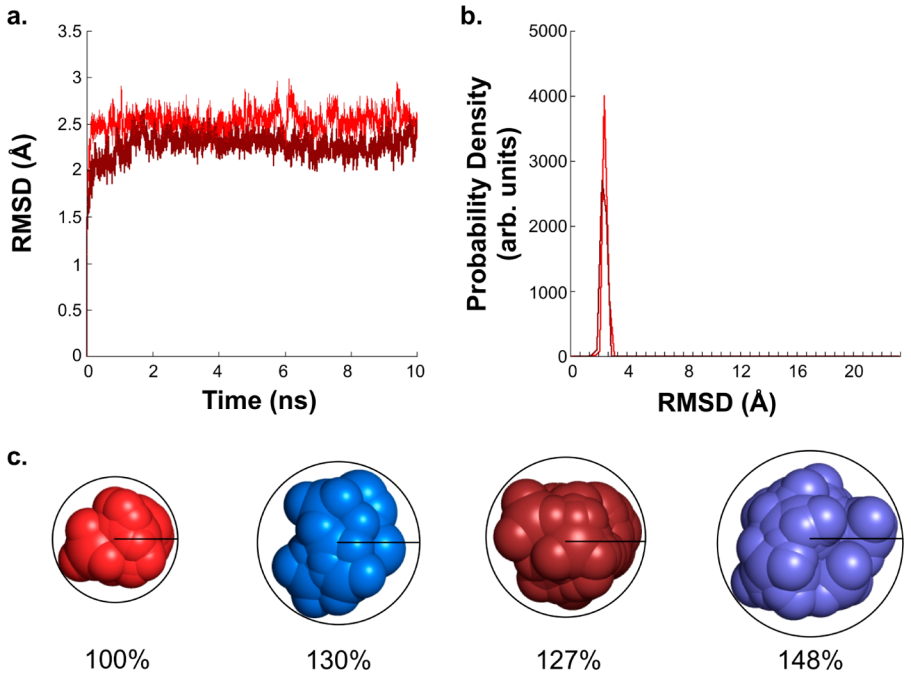

Figure 15. Dynamic behavior for the 4T-SGQs $\mathbf{1}_{16}$ (red) and $\mathbf{2}_{16}$ (burgundy). (a) Evolution of the RMSD (relative to the NMR-based minimized structure) as a function of time and (b) the corresponding distributions for both SGQs. (c) Superposition of the methyl and ethoxy groups corresponding to multiple configurations of the subunits in the outer (red/burgundy) and inner (light blue/light purple) tetrads in $\mathbf{1}_{16}$ and $\mathbf{2}_{16}$. The percentages were computed by normalizing the indicated radii to the one corresponding to the methyl groups (red) in the outer tetrads of $\mathbf{1}_{16}$.

pyridyl)-*d*G-derivative, which engages in enough attractive interactions (i.e., dipole−dipole) to stabilize this particular molecularity, but not enough to stabilize a 4T-SGQ.[54]

At the molecular level, in $\mathbf{1}_{16}$, neither the sugar pucker nor the angles of each subunit **1** changes significantly during the duration of the MD simulations. Furthermore, during this period the pattern of H-bonds remains fairly constant with a nonsymmetrical arrangement for tetrads (Figure 14c−d). Although, all the tetrads become more concave, this phenomenon is more pronounced for the solvent-exposed outer tetrads, which have greater degrees of freedom (Figure S25). Formation of additional H-bonds between the *meta*-carbonyl group at the C8-phenyl group and the N2H pointing to the groove edge, clamp the outer and inner tetrads together, as predicted by the initial 3-D model (Figure 11e).

Additional MD simulations were performed for $\mathbf{2}_{16}$ (Figure S27−29) in order to gain a better understanding of the impact in the resulting SGQ for replacing a *meta*-acetyl (**1**) with a *meta*-ethoxycarbonyl (**2**). Simulations of both $\mathbf{1}_{16}$ and $\mathbf{2}_{16}$ reveal similar trajectories and distribution peaks (ca. 2.5 Å), but with the latter showing slightly lower RMSD values (Figure 15). A close inspection at the evolution of the structures of $\mathbf{1}_{16}$ and $\mathbf{2}_{16}$ throughout the simulations reveal that the central core of the former is more compact than that of the latter. This agrees with our previously reported hypothesis that the increased steric bulk imposed by the bigger ethoxy groups shifts the equilibrium from $\mathbf{2}_{16}$ to the corresponding octamer $\mathbf{2}_8$.[55] Despite the presence in **2** of the presumably better H-bond donor carbonyl of the ester, relative to the ketone in **1**, this enhanced steric repulsion also resulted in $\mathbf{2}_{16}$ being thermally less stable (by 6 K) than $\mathbf{1}_{16}$ (as determined by variable temperature NMR).[55] Furthermore, these results also support our previously proposed mechanism of formation for hexadecamers (4T-SGQ).[55] Specifically, we hypothesized that, unlike other hexadecamers reported in the literature,[24] the 4T-SGQs made by 8ArG derivatives resulted from the dimerization of two octamers (2T-SGQ) in a process promoted by the greater availability of the cation template (e.g., K^+).

A close inspection of several structures throughout the trajectory allows the identification of key interactions and structural details that affect the stability of the resulting assemblies. For example, the bifurcated hydrogen bonds clamp the subunits in the outer tetrads to those in the inner tetrads, increasing the overall stability of the system (Figure 11e). These clamping interactions, however, lead to a detrimental entropic penalty because of the reduced degrees of freedom of the acetyl, or ethoxycarbonyl, groups in the outer tetrads. This is seen in the apparent lower mobility of the groups (methyl/ethoxy) attached to the meta-carbonyl moieties, which occupy a smaller hydrodynamic volume (Figure 15c, red/burgundy) relative to those of the inner tetrads (Figure 15c, blue/purple).

Additional MDS studies with the SGQs formed by the *para*-substituted derivative **3** ($\mathbf{3}_8$, $\mathbf{3}_{12}$ and $\mathbf{3}_{16}$) provide further insight into the origins of the differences in supramolecular properties relative to the *meta*-substituted **1** (Figures 16, S30). In general, and similar to the SGQs formed by **1** and **2**, $\mathbf{3}_8$, $\mathbf{3}_{12}$, and $\mathbf{3}_{16}$ show negligible changes in the sugar pucker, and the angles of the individual subunits. There is an increase, however, in the length of the H-bonds and they assume a nonsymmetrical arrangement during the same period. While $\mathbf{3}_8$ appears to shows the lowest and narrowest RMSD distribution (Figure 16b), after 2 ns, there is a sudden increase in the RMSD trajectory that results from a loss in planarity of the tetrads. The latter is not necessarily surprising since the two tetrads are solvent exposed and therefore have more freedom relative to the inner tetrads in $\mathbf{3}_{16}$. RMSD spread for all three SGQs is not large (2−5 Å), which is similar to $\mathbf{1}_{16}$ and $\mathbf{1}_8$. While the RMSD for $\mathbf{3}_{12}$ is also in this range, this is in sharp contrast to $\mathbf{1}_{12}$, which has a very broad distribution with 1 order of magnitude higher RMSD. Given the narrow range of RMSD distributions for all

DOI: 10.1021/acs.joc.6b01113
J. Org. Chem. 2016, 81, 6026−6035

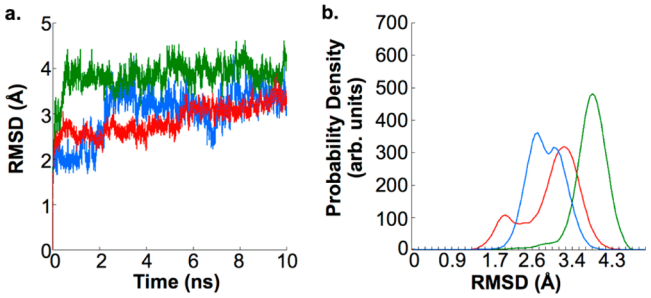

Figure 16. Dynamic behavior for of $\mathbf{3}_{16}$ (red), $\mathbf{3}_{12}$ (green), and $\mathbf{3}_{8}$ (blue). (a) Evolution of the RMSD (relative to the NMR-based minimized structure) as a function of time and (b) the corresponding distributions for the three SGQs.

SGQs made by **3**, it would be reasonable to expect to have a mixture of equilibrating species in solution (i.e., $\mathbf{3}_{8}$, $\mathbf{3}_{12}$, and $\mathbf{3}_{16}$). However, only $\mathbf{3}_{8}$ is formed with good fidelity as it is the only experimentally detected species by NMR (Figure S18). What prevents the system from forming the higher ordered SGQs? Entropy should disfavor the formation of $\mathbf{3}_{12}$ and $\mathbf{3}_{16}$ due to the absence of strongly stabilizing attractive interactions (enthalpic compensation), such as those possible in $\mathbf{1}_{16}$ with the *meta*-carbonyl group.

CONCLUSION

Although the 3-D structure of 4T-SGQs formed by various lipophilic guanosine derivatives (with no substitution at the C8) have been previously reported,[19,43,44] up to this date there have been no reports of a detailed structural study for the corresponding 4T-SGQs formed by 8-phenyl-substituted G-derivatives. Combining NMR and MDS studies, we have established a detailed picture of the structure of 4T-SGQs formed by three different derivatives with *meta*-carbonylphenyl groups (**1**, **1a**, and **2**) and contrasted their properties to one with *para*-carbonyl substitution (**3**) that forms instead a 2T-SGQ. The experimental evidence supports that in all cases, of the four possible D_4-symmetric 4T-SGQs, only the one with the interfacial configurations of *ht-hh-th* is formed. The reasons for the high stereoselectivity and fidelity results from the synergistic combination of multiple noncovalent interactions that lead to a highly cooperative assembly and allosteric effects in these 4T-SGQs. Furthermore, these properties in turn enable the isostructural assembly of the related lipophilic (**1**) and hydrophilic (**1a**) derivatives in both organic and aqueous media, respectively. The attractive interactions within these 4T-SGQs act in concert with repulsive steric and electronic interactions that prevent the solvent-exposed outer tetrads from "accepting" the assembly of further tetrads, which prevents the formation of the columnar aggregates (*n*T-SGQs). This self-terminating property is relatively uncommon for an open supramolecule, but provides a powerful platform for the construction of functional assemblies with potential applications in materials science and biomedicine.[50,56]

EXPERIMENTAL SECTION

General. Compound **1** was synthesized and purified as previously reported.[31] NMR spectra were recorded on spectrometers equipped with either a 5 mm BBO or a TXI probe, with nominal frequencies of 500.13 MHz for proton and 125 MHz for carbon, respectively.

Sample Preparation for NMR Studies. Self-assembly studies were performed for example using a 30−40 mM solution of the analogue in 600 μL of CD_3CN and 0.5 equiv of KI. Self-assembly studies in water were performed using a 10 mM solution of **1a** in 600 μL of H_2O-D_2O (9:1).

NMR Spectroscopy. For the COSY standard gradient base 2D pulse sequence were used. 2D NOESY experiments were collected in a gradient base phase-sensitive mode with a mixing time of 500 ms. For the experiments in water, 1D ^1H NMR was performed with a presaturation pulse sequence with the excitation pulse set over the water peak at 4.7 ppm. For the NOESY experiments a phase-sensitive 2D NOESY pulse sequence with presaturation (noesyphpr) was used. All NMR experiments were performed at 298 K unless otherwise stated.

Molecular Modeling and Molecular Dynamics Simulations. Initially, the structures of all the monomers were constructed using Maestro 8.0.315.[34] These monomers were used for building the various SGQs that were manually assembled. The coordinates for these initial configurations were in accordance with the structural information obtained from the 2D NOESY spectra of the various SGQs studied in our laboratory. Energy minimizations were performed to these initially constructed supramolecular structures using the MacroModel suite of programs employing the AMBER 94 force field.[34]

From these optimized structures two different configurations of the monomer (the structure of the monomer on the outer and the inner tetramers) were used to derive electrostatic charges using the standard procedure for the AMBER force field, as implemented in RED III.[35−37] Briefly, the procedure followed the following steps: (i) each monomer was optimized using the HF/6-31G* method, from the Gaussian 03 package; (ii) frequency calculations were performed to verify the identity of each stationary point as a minimum; (iii) this minimized structure was used to obtain the charges of each atom using ESP software. In this calculation the charges corresponding to the sugar and the guanine base were fixed according to the force field. When the AMBER force field parameters were not available for particular atoms, the GAFF force filed parameters were used.[38]

One, two, and three cations were placed between consecutive tetrads using Maestro.[34] Xleap was used to import the pdb and add the corresponding Cl^- atoms, using the addions2 command, to neutralize the system. A 10 Å truncated octahedron, with a minimum distance of 10 Å from the molecular surface to the boundaries surface (using CH_3CN as solvent), was added to solvate the structure giving a total system of approximately 4,704 atoms in the case of a hexadecamer (4T-SGQ). The molecular dynamics simulations were carried out using the AMBER 10 suite of programs with AMBER-99SB as modified by Sponer.[39] The atoms in the simulation were given a 12 Å cutoff and the particle mesh Ewald method was implemented to treat the long-range electrostatics and to reduce the negative effects of the introduction of a cutoff. The temperature and pressure were fixed 300 K and 1 atm, respectively. SANDER was used to carry out the minimizations and the molecular dynamics runs. The total simulation time ranged from 10 to 30 ns, depending on the system. Usually, when the root-mean-square deviation (RMSD) reached constant values the simulation was concluded. VMD was used for graphical representations of the generated trajectories.[40] As in previous studies,[30a] the variation of RMSD as a function of time was used as a measurement of the stability of the system. Specifically, increments in RMSD values imply a deviation from the initial structure, which in this study was based on 2D NOESY information. As the deviation increases, the system diverges more from the experimental structure, which is interpreted as being less stable.

For the statistical analysis, histogram plots of the distribution of the root-mean-square displacements for all the structures were generated using a maximum number of counts of 4500 for all the structures, with bin sizes of 70.

ASSOCIATED CONTENT

Supporting Information

The Supporting Information is available free of charge on the ACS Publications website at DOI: 10.1021/acs.joc.6b01113.

Additional NMR spectra (PDF)

DOI: 10.1021/acs.joc.6b01113
J. Org. Chem. 2016, 81, 6026−6035

Crystallographic data (CIF)
Molecular models (PDB)
Molecular models (PDB)
Molecular models (PDB)
Molecular models (PDB)
Molecular models (PDB)
Molecular models (PDB)
MDS data (ZIP)

AUTHOR INFORMATION

Corresponding Author

*E-mail: riveralab.upr@gmail.com

Notes

The authors declare no competing financial interest.

ACKNOWLEDGMENTS

This research was financially supported by the NIH-SCoRE (Grant No. 5SC1GM093994). M.G.A. thanks the NIH-RISE Program (2R25GM061151) and NSF-EPSCoR (EPS0223152) for graduate fellowships.

REFERENCES

(1) Chi, X.; Guerin, A. J.; Haycoc, R. A.; Hunter, C. A.; Sarson, L. D. *J. Chem. Soc., Chem. Commun.* **1995**, 2563−2565.

(2) The dimensionality attributed to an object depends on the (mental or physical) operations performed on it. Thus, it is a matter of convenience and not a fundamental property of the object itself. For example, a 2-D object in the low end of the nanoscale looks as a 0-D object at higher magnification. (a) Kaye, B. H. *A random walk through fractal dimensions*; Wiley Online Library: New York, 1989. (b) Mandelbrot, B. B. How Long is the Coast of Britain: Statistical Self-similarity and Fractal Dimension. *Science* **1967**, *156*, 636−638.

(3) Goodsell, D. S.; Olson, A. J. *Annu. Rev. Biophys. Biomol. Struct.* **2000**, *29*, 105−153.

(4) Keizer, H. M.; Sijbesma, R. P. *Chem. Soc. Rev.* **2005**, *34*, 226−234.

(5) Kato, T.; Mizoshita, N.; Kishimoto, K. *Angew. Chem., Int. Ed.* **2006**, *45*, 38−68.

(6) Jin, S.; Ma, Y.; Zimmerman, S. C.; Cheng, S. *Chem. Mater.* **2004**, *16*, 2975−2977.

(7) Suárez, M.; Lehn, J.-M.; Zimmerman, S. C.; Skoulios, A.; Heinrich, B. *J. Am. Chem. Soc.* **1998**, *120*, 9526−9532.

(8) Palmer, L. C.; Stupp, S. I. *Acc. Chem. Res.* **2008**, *41*, 1674−1684.

(9) Dankers, P. Y. W.; Meijer, E. W. *Bull. Chem. Soc. Jpn.* **2007**, *80*, 2047−2073.

(10) Jun, H.; Paramonov, S. E.; Hartgerink, J. D. *Soft Matter* **2006**, *2*, 177−181.

(11) Zhang, S. *Nat. Biotechnol.* **2003**, *21*, 1171−1178.

(12) Brunsveld, L.; Folmer, B. J. B.; Meijer, E. W.; Sijbesma, R. P. *Chem. Rev.* **2001**, *101*, 4071−4097.

(13) Hoeben, F. J. M.; Jonkheijm, P.; Meijer, E. W.; Schenning, A. P. H. J. *Chem. Rev.* **2005**, *105*, 1491−1546.

(14) Park, T.; Zimmerman, S. C. *J. Am. Chem. Soc.* **2006**, *128*, 13986−13987.

(15) Besenius, P.; Portale, G.; Bomans, P. H. H.; Janssen, H. M.; Palmans, A. R. A.; Meijer, E. W. *Proc. Natl. Acad. Sci. U. S. A.* **2010**, *107*, 17888−17893.

(16) Besenius, P.; van den Hout, K. P.; Albers, H. M. H. G.; De Greef, T. F. A.; Olijve, L. L. C.; Hermans, T. M.; de Waal, B. F. M.; Bomans, P. H. H.; Sommerdijk, N. A. J. M.; Portale, G.; Palmans, A. R. A.; Van Genderen, M. H. P.; Vekemans, J. A. J. M.; Meijer, E. W. *Chem. - Eur. J.* **2011**, *17*, 5193−5203.

(17) De Greef, T. F. A.; Smulders, M. M. J.; Wolffs, M.; Schenning, A. P. H. J.; Sijbesma, R. P.; Meijer, E. W. *Chem. Rev.* **2009**, *109*, 5687−5754.

(18) Examples of 2D supramolecules include lamellar structures, self-assembled monolayers, membranes and surface assemblies (a) Love, J. C.; Estroff, L. A.; Kriebel, J. K.; Nuzzo, R. G.; Whitesides, G. M. *Chem. Rev.* **2005**, *105*, 1103−1169. (b) Ulman, A. *Chem. Rev.* **1996**, *96*, 1533−1554. While 3D supramolecules include crystalline solids and metal−organic frameworks (MOFs). Cook, T. R.; Zheng, Y.-R.; Stang, P. J. *Chem. Rev.* **2013**, *113*, 734−777.

(19) González-Rodríguez, D.; van Dongen, J. L. J.; Lutz, M.; Spek, A. L.; Schenning, A. P. H. J.; Meijer, E. W. *Nat. Chem.* **2009**, *1*, 151−155.

(20) Smulders, M. M. J.; Nieuwenhuizen, M. M. L.; Grossman, M.; Filot, I. A. W.; Lee, C. C.; De Greef, T. F. A.; Schenning, A. P. H. J.; Palmans, A. R. A.; Meijer, E. W. *Macromolecules* **2011**, *44*, 6581−6587.

(21) In nature capping proteins are used to control the aggregation of actin: Pollard, T. D.; Blanchoin, L.; Mullins, R. D. *Annu. Rev. Biophys. Biomol. Struct.* **2000**, *29*, 545−576. or by the use of template effects: (a) Hunter, C. A.; Tomas, S. *J. Am. Chem. Soc.* **2006**, *128*, 8975−8979. (b) Bull, S. R.; Palmer, L. C.; Fry, N. J.; Greenfield, M. A.; Messmore, B. W.; Meade, T. J.; Stupp, S. I. *J. Am. Chem. Soc.* **2008**, *130*, 2742−2743.

(22) In the following two references the authors report a partial control of the extent of the assembly by introducing electrostatic repulsion: (a) Besenius, P.; Portale, G.; Bomans, P. H. H.; Janssen, H. M.; Palmans, A. R. A.; Meijer, E. W. *Proc. Natl. Acad. Sci. U. S. A.* **2010**, *107*, 17888−17893. (b) Besenius, P.; van den Hout, K. P.; Albers, H. M. H. G.; De Greef, T. F. A.; Olijve, L. L. C.; Hermans, T. M.; de Waal, B. F. M.; Bomans, P. H. H.; Sommerdijk, N. A. J. M.; Portale, G.; Palmans, A. R. A.; Van Genderen, M. H. P.; Vekemans, J. A. J. M.; Meijer, E. W. *Chem. - Eur. J.* **2011**, *17*, 5193−5203 Changing the solvent has also enabled this as described in ref 19.

(23) In here we use the term SGQs to refer to supramolecular G-quadruplexes and distinguish them from oligonucleotide based G-quadruplexes or OGQs. For more details see: Rivera, J. M. Functional assemblies made from supramolecular G-quadruplexes. In *Guanine quartets: Structure and application*; Spindler, L., Fritzsche, W., Eds.; RSC Publishing: Cambridge, U.K., 2012.

(24) (a) Davis, J. T.; Spada, G. P. *Chem. Soc. Rev.* **2007**, *36*, 296−313. (b) Davis, J. T. *Angew. Chem., Int. Ed.* **2004**, *43*, 668−698.

(25) Spada, G. P.; Gottarelli, G. *Synlett* **2004**, 596−602.

(26) Abet, V.; Rodriguez, R. *New J. Chem.* **2014**, *38*, 5122−5128.

(27) (a) Mezzina, E.; Mariani, P.; Itri, R.; Masiero, S.; Pieraccini, S.; Spada, G. P.; Spinozzi, F.; Davis, J. T.; Gottarelli, G. *Chem. - Eur. J.* **2001**, *7*, 388−395. (b) Forman, S. L.; Fettinger, J. C.; Pieraccini, S.; Gottarelli, G.; Davis, J. T. *J. Am. Chem. Soc.* **2000**, *122*, 4060−4067.

(28) We treat SGQs as assemblies of *n*-tetrads (*n*T) in which, for example, an octameric SGQ (composed of two tetrads) is referred to as a 2T-SGQ. Similarly, a dodecamer is a 3T-SGQ and a hexadecamer is 4T-SGQ. The nomenclature, however, does not imply that the mechanism of assembly/disassembly occurs via the oligomerization of preformed tetrads, although that possibility cannot be discarted.

(29) For reports on the use of such aggregates in the preparation of hydrogels see: (a) Chantot, C. F.; Guschlbauer, W. In *Mechanism of Gel Formation by Guanine Nucleosides, The Purines; Theory and Experiment*, Jerusalem, 4−8 April 1971; Jerusalem, 1972, pp 205−216. (b) Bang, I. *Biochem. Z.* **1910**, *26*, 293. (c) Sreenivasachary, N.; Lehn, J. M. *Proc. Natl. Acad. Sci. U. S. A.* **2005**, *102*, 5938−5943. (d) Ghoussoub, A.; Lehn, J. M. *Chem. Commun.* **2005**, *46*, 5763−5765. (e) Peters, G. M.; Skala, L. P.; Plank, T. N.; Oh, H.; Manjunatha Reddy, G. N.; Marsh, A.; Brown, S. P.; Raghavan, S. R.; Davis, J. T. *J. Am. Chem. Soc.* **2015**, *137*, 5819−5827. (f) Peters, G. M.; Skala, L. P.; Plank, T. N.; Hyman, B. J.; Manjunatha Reddy, G. N.; Marsh, A.; Brown, S. P.; Davis, J. T. *J. Am. Chem. Soc.* **2014**, *136*, 12596−12599. In the development of liquid crystals see: (g) Spada, G. P.; Gottarelli, G. *Synlett* **2004**, *4*, 596−602. Pieraccini, S.; Giorgi, T.; Gottarelli, G.; Masiero, S.; Spada, G. P. *Mol. Cryst. Liq. Cryst.* **2003**, *398*, 57−73.

(30) (a) Martín-Hidalgo, M.; García-Arriaga, M.; González, F.; Rivera, J. M. *Supramol. Chem.* **2015**, *27*, 174−180. (b) Martín-Hidalgo, M.; Rivera, J. M. *Chem. Commun.* **2011**, *47*, 12485−12487. (c) Martín-Hidalgo, M.; Camacho-Soto, K.; Gubala, V.; Rivera, J. M. *Supramol. Chem.* **2010**, *22*, 862−869.

(31) Gubala, V.; Betancourt, J. E.; Rivera, J. M. *Org. Lett.* **2004**, *6*, 4735−4738.

DOI: 10.1021/acs.joc.6b01113
J. Org. Chem. 2016, 81, 6026−6035

(32) García-Arriaga, M.; Hobley, G.; Rivera, J. M. *J. Am. Chem. Soc.* **2008**, *130*, 10492−10493.
(33) We have taken advantage of this property to develop functional assemblies with precise structures such as thermosensitive supramolecules and self-assembled dendrimers. For examples see ref 50 and 56 and Rivera, L. R.; Betancourt, J. E.; Rivera, J. M. *Langmuir* **2011**, *27*, 1409−1414.
(34) *MacroModel*, Version 9.5, Maestro 8.0.315 ed.; Schrödinger, LLC: New York, 2007.
(35) Cieplak, P.; Cornell, W. D.; Bayly, C.; Kollman, P. A. *J. Comput. Chem.* **1995**, *16*, 1357−1377.
(36) Dupradeau, F. Y.; Pigache, A.; Zaffran, T.; Savineau, C.; Lelong, R.; Grivel, N.; Lelong, D.; Rosanski, W.; Cieplak, P. *Phys. Chem. Chem. Phys.* **2010**, *12*, 7821−7839.
(37) Cornell, W. D.; Cieplak, P.; Baily, C. I.; Gould, I. R.; Merz, K. M.; Ferguson, D. C.; Fox, T.; Caldwell, J. W.; Kollman, P. A. *J. Am. Chem. Soc.* **1995**, *117*, 5179−5197.
(38) Wang, J.; Wolf, R. M.; Caldwell, J. W.; Kollman, P. A.; Case, D. A. *J. Comput. Chem.* **2004**, *25*, 1157−1174.
(39) Pearlman, D. A.; Case, D. A.; Caldwell, J. W.; Ross, W. S.; Cheatham, T. E.; DeBolt, S.; Ferguson, D.; Seibel, G.; Kollman, P. *Comput. Phys. Commun.* **1995**, *91*, 141.
(40) Humphrey, W.; Dalke, A.; Schulten, K. *J. Mol. Graphics* **1996**, *14*, 33−38.
(41) Marlow, A.; Mezzina, E.; Spada, G. P.; Masiero, S.; Davis, J. T.; Gottarelli, G. *J. Org. Chem.* **1999**, *64*, 5116−5123.
(42) See Figure 3 for the definition of the head and tail concepts.
(43) Wu, G.; Wong, A.; Gan, Z.; Davis, J. *J. Am. Chem. Soc.* **2003**, *125*, 7182−7183.
(44) Wu, G.; Gan, Z.; Kwan, I. C. M.; Fettinger, J. C.; Davis, J. T. *J. Am. Chem. Soc.* **2011**, *133*, 19570−19573.
(45) Assignment of outer (o) and inner (i) tetrads is based on the upfield chemical shift expected for the inner tetrads. This is owing to the anisotropic shielding effect created by the aromatic rings of the outer tetrads.
(46) Millen, A. L.; Manderville, R. A.; Wetmore, S. D. *J. Phys. Chem. B* **2010**, *114*, 4373−4382.
(47) The letter *w* is used to identify the N_2H hydrogen facing the Watson−Crick edge of the guanine and *g* is used for the one pointing towards the groove edge.
(48) Reshetnikov, R.; Golovin, A.; Spiridonova, V.; Kopylov, A.; Sponer, J. *J. Chem. Theory Comput.* **2010**, *6*, 3003−3014.
(49) There are a number of articles in the literature that report intertetrad twist angles with different definitions, the values reported in here were determined following Sponer's definition (ref 48).
(50) (a) Betancourt, J. E.; Rivera, J. M. *J. Am. Chem. Soc.* **2009**, *131*, 16666−16668. (b) Negrón, L. M.; Meléndez-Contés, Y.; Rivera, J. M. *J. Am. Chem. Soc.* **2013**, *135* (10), 3815−3817. (c) Betancourt, J. E.; Rivera, J. M. *Langmuir* **2015**, *31*, 2095−2103.
(51) In CD_3CN **2** forms almost exclusively a *4*T-SGQ, which is the basis for the solvo-responsive system described earlier by our group in reference 55.
(52) This phenomenon can be attributed to a through-space effect of the acetyl group on the phenyl ring and not necessarily to a resonance effect as described in: Wheeler, S. E.; Houk, K. N. J. *J. Chem. Theory Comput.* **2009**, *5*, 2301−2312.
(53) Gubala, V. Ph.D. Dissertation; University of Puerto Rico: Río Piedras 2006.
(54) Rivera-Sánchez, M. d. C.; Andújar-de-Sanctis, I.; García-Arriaga, M.; Gubala, V.; Hobley, G.; Rivera, J. M. *J. Am. Chem. Soc.* **2009**, *131*, 10403−10405.
(55) Betancourt, J. E.; Martín-Hidalgo, M.; Gubala, V.; Rivera, J. M. *J. Am. Chem. Soc.* **2009**, *131*, 3186−3188.
(56) (a) Rivera, J. M.; Martín-Hidalgo, M.; Rivera-Ríos, J. C. *Org. Biomol. Chem.* **2012**, *10*, 7562−7565. (b) Betancourt, J. E.; Subramani, C.; Serrano-Velez, J. L.; Rosa-Molinar, E.; Rotello, V. M.; Rivera, J. M. *Chem. Commun.* **2010**, *46*, 8537−8539.

DOI: 10.1021/acs.joc.6b01113
J. Org. Chem. 2016, 81, 6026−6035